X-Ray diffraction line broadening by stacking faults in SrBi2Nb2O9/SrTiO3 epitaxial thin films

Alexandre Boulle, Caroline Legrand, Jean-Pierre Mercurio, René Guinebretière, Alain Dauger

X-Ray diffraction line broadening by stacking faults in $SrBi_2Nb_2O_9/SrTiO_3$ epitaxial thin films

A. Boulle[a], C. Legrand[b], R. Guinebretière[a,*], J.P. Mercurio[b], A. Dauger[a]

[a] *ENSCI, 47-73 avenue Albert Thomas, 87065 Limoges Cedex, France*
[b] *Faculté des Sciences, 123 avenue Albert Thomas, 87060 Limoges Cedex, France*

$SrBi_2Nb_2O_9$ thin films were deposited on (001) $SrTiO_3$ substrate by sol–gel spin coating. A previous study showed that the film crystallizes with the *c*-axis normal to the surface. Those epitaxial films are studied by means of X-ray diffraction (XRD) line profile analysis as a function of thermal annealing duration. The line profile analysis of the diffraction patterns collected in ω-2θ scan mode, gives detailed information on the coherently diffracting domain size and microstrains along a given direction. For low annealing duration the width of the (001) diffraction lines reaches values of approximately 1°. In accordance with a recent study, integral breadth and Fourier analysis suggest the presence of stacking faults separated by a mean distance of 5 nm. The profiles exhibit a marked Lorentzian character as expected from a faulted crystal. In addition to faulting, both finite grain size and microstrains contribute to the observed width. When heat treatment time is increased, the breadth and Lorentzian content of the (001) diffraction lines decrease attesting that the stacking fault density is lowered. For a 500-h treatment at 700°C the calculated domain size equals the films thickness. This indicates that stacking faults have almost disappeared: the SBN crystallites of the film have reached an equilibrium state.

Keywords: Epitaxy; Line profile analysis; X-Ray diffraction; Layered pevovskite

1. Introduction

Ferroelectric thin films have been widely investigated in the past decade for potential application in non-volatile random access memories (NVRAM). Aurivillius compounds are a family of bismuth containing perovskites which have been reported to have good fatigue resistance. Those compounds are hence very attractive for NVRAM applications [1]. The Aurivillius compound $SrBi_2Nb_2O_9$ (SBN) is made of the stacking of $[Sr_{m-1}Nb_mO_{3m+1}]^{2-}$ perovskite blocks with a layer thickness of $m = 2$, separated by $[Bi_2O_2]^{2+}$ slabs [2] (see also Fig. 1). Other members of this family show an m value ranking between 1 and 5. In those layered compounds stacking faults (a local variation of the m value) are very likely to occur. Those types of stacking faults, with local chemical content changes, have been reported in SBN compounds [3], in similar bismuth containing oxides [4], and in the widely studied perovskite like $YBa_2Cu_3O_{7-\delta}$ [5–7].

The stacking fault density is an important parameter since the ferroelectric properties, especially polarization and coercive field are tightly bound to the thickness of the perovskite layer [8]. It has been shown that such stacking faults produce X-ray diffraction (XRD) line broadening [3]. XRD is a widely used tool for thin film analysis, especially because of the statistical relevance of the data and its non-destructive character. The purpose of this paper is to proceed to a mi-

* Corresponding author. Tel.: +33-5-55-45-22-21; fax: +33-5-55-79-09-98.
E-mail address: r.guinebretiere@ensci.fr (R. Guinebretière).

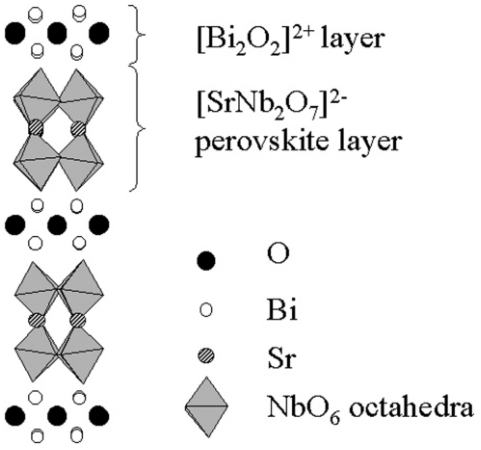

Fig. 1. Projection of $SrBi_2Nb_2O_9$ oriented along the $0x$ axis.

crostructural analysis of epitaxial SBN thin films deposited on $SrTiO_3$ substrates using X-ray diffraction line profile analysis.

2. Experimental

2.1. Material synthesis

Thin films were fabricated by spinning a sol–gel precursor solution at 4000 rev./min for 30 s onto single crystalline (001) $SrTiO_3$ substrates using a Sulzer photoresist spinner. The precursor solution was prepared the following way: (i) dissolution of strontium 2-ethylhexanoate in 2-ethylhexanoic acid at 120°C; (ii) addition of bismuth 2-ethylhexanoate; and (iii) addition of niobium ethoxide dissolved in ethanol.

The films are dried in an electric oven at 300°C for 10 min before being thermally annealed at 700°C for 30 min, 2 h and 500 h.

2.2. Data collection

X-Ray diffraction experiments were performed on a home made high-resolution set-up [9]. The primary linear beam is supplied by a rotating anode source (Bruker AXS). A four-reflection monochromator made of two Ge(220) channel cut crystals provides high collimation ($\Delta\theta = 12''$) and monochromatization ($\Delta\lambda/\lambda = 1.4 \times 10^{-4}$) of the incident beam. Diffracted beams are collected over 120° using a curved position sensitive detector (INEL CPS120). Samples were positioned on a five-axis sample holder in a vacuum chamber. Precise sample positioning is performed by using the diffracted beams of the substrate [10]. One of the particular features of this set-up is its high versatility since with the same data set we are able to obtain ω-2θ scans, ω scans, rocking curves and reciprocal space maps.

In order to perform line profile analysis on epitaxial thin films, samples are studied in ω-2θ scan mode [3]. In this method, the crystal is rocked through the Bragg law setting of a given reflection. The angular rocking range ($\omega\max - \omega\min$) is chosen wide enough to include everything from the reflection. For each incidence angle ω diffracted beams are collected over a range of $2\theta = 120°$. The final diffraction line is built up using the following equation:

$$I(2\theta) = \int_{\omega\min}^{\omega\max} k(\omega) I(\omega, 2\theta) \mathrm{d}\omega \quad (1)$$

where $I(\omega,2\theta)$ is the intensity recorded at 2θ for the incidence angle ω; the factor $k(\omega)$ allows for geometrical corrections (irradiated volume, absorption...).

3. Line profile analysis

Microstructural information can be obtained from the analysis of diffraction line broadening [11]. However, for reliable parameters to be extracted the diffraction lines must be perfectly modeled, especially in the tails of the profile. A Voigt function (i.e. the convolution of a Lorentzian and a Gaussian function) [12] was used to model the line profiles; the peak position, peak area and integral breadth β_G and β_L were refined. The form factor ϕ is the ratio of the full width at half maximum to the integral breadth ($\phi = \mathrm{FWHM}/\beta$); it describes the shape of the profile. It has limiting values of 0.636 and 0.939 for a Lorentzian and a Gaussian function, respectively.

The Voigt function is convoluted with the instrumental profile [9] so that the refined parameters correspond to the sample contribution to line broadening. Two methods of line broadening analysis are widely used.

Integral breadth analysis: in the method introduced by Langford [12,13] the Lorentzian (β_L) and Gaussian (β_G) components expressed in reciprocal space ($\beta^* = \beta\cos\theta/\lambda$) are analyzed separately as a function of the diffraction vector:

$$\beta_L^* = \beta_{s_L}^* + \frac{\eta_L}{2} d^*$$

$$\beta_G^{*2} = \beta_{s_G}^{*2} + \left(\frac{\eta_G}{2}\right)^2 d^{*2}$$

where the subscript s refers to the size contribution to line breadth and $d^* = 2\sin\theta/\lambda$ is the length of the diffraction vector. Plotting β_L^* vs. d^* and β_G^{*2} vs. d^{*2} yields β_{s_L}, β_{s_G} derived from the intercepts, and η_L, η_G from the slopes which allows to separate the volume averaged domain size $\langle D \rangle_v$ and the apparent strain η [13].

Fourier analysis: the convolution fitting procedure described above combined with the Warren–Averbach method [14] enables us to avoid the usual scheme of

Stokes deconvolution [15] which often leads to spurious effects or unstable solutions [16–18]. Hence the Fourier coefficients of the line profile are given by those of the Voigt function representing the physically broadened profile:

$$A(L) = \exp(-2L\beta_L^* - \pi L^2 \beta_G^{*2})$$

where L is the column length. The size coefficient $As(L)$ and mean squared strain $\langle e^2(L)\rangle$ can be separated by means of the following equation [19]:

$$A(L) = As(L)(1 - 2\pi^2 d^{*2} L^2 \langle e^2(L)\rangle)$$

The column length distribution $p(L)$ is obtained from the second derivative of the cosine size coefficient $As(L)$ [20]:

$$p(L) \propto L \frac{\mathrm{d}^2 As(L)}{\mathrm{d}L^2}$$

The above mentioned methods require at least two orders of reflection of the same crystallographic plane family. Owing to the high value of the SBN c parameter ($c = 25.1124$ Å, see JCPDS card 86-1190) this condition is easily fulfilled.

4. Results and discussion

The process described in Section 2 leads to c-oriented $SrBi_2Nb_2O_9$ on $SrTiO_3$ such as $(001)_{SBN}//(001)_{ST}$ and $[100]_{SBN}//[110]_{ST}$ [21]. A reciprocal space map close to the (004) line of a 2-h annealed SBN thin film is given in Fig. 2. The reciprocal lattice node is markedly broadened in the direction parallel to the diffraction vector. This high anisotropy suggests the presence of defects along the c-axis. According to Aurivillius [2] this anisotropy may be due to stacking faults. However, microstrains may also contribute to line broadening.

Several (001) lines were recorded in ω-2θ scan mode. The (0010) line reconstructed by means of Eq. (1) of a SBN thin film heat-treated at 700°C for 2 h is depicted in Fig. 3. In Fig. 4 we plotted the integral breadths of the physically broadened profiles vs. d^* in a Williamson–Hall plot [22]. It is clear from this figure that both stacking faults and microstrains contribute to the observed width [3]. In order to separate more accurately these two contributions the data were analyzed by the Langford method [13] and the Fourier method described above. The calculation yields a volume weighted domain size of 7.4 (1) nm for the sample annealed for 30 min. The apparent strain η has a value of 3.1 (1)%. All results are given in Table 1 for three different annealing durations. $\langle D\rangle_v$ and $\langle D\rangle_s$ are the volume and surface averaged domain sizes calculated

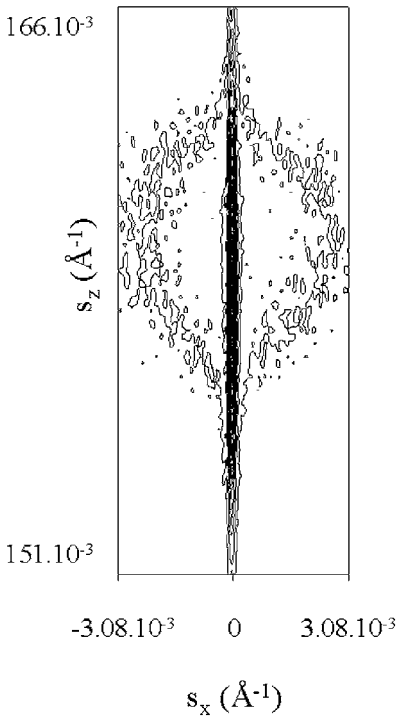

Fig. 2. Reciprocal space map close to the (004) reflection of a $SrBi_2Nb_2O_9$ epitaxial thin film annealed 2 h at 700°C. Sz is parallel to $[001]^*_{SBN}$ and Sx is parallel to $[110]^*_{SBN}$.

with the Langford and Warren–Averbach methods, respectively. η is the apparent strain calculated with the Langford method, whereas $\langle e^2\rangle^{1/2}$ is the root mean squared strain calculated at $\langle D\rangle_s/2$ with the Warren–Averbach method. Finally the shape factors $\langle\phi\rangle$ and ϕ_D (for details see below) are given.

Defects consisting of coherently diffracting domains shifted with respect to each other (which in SBN corresponds to a local variation of the m value) has been described by van Berkum et al. as highly localized strain fields [23]. The corresponding line profiles exhibit

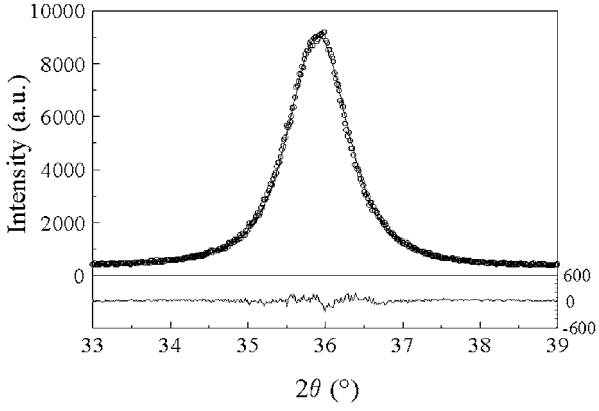

Fig. 3. (0010) Diffraction line reconstructed by means of Eq. (1) of a $SrBi_2Nb_2O_9$ epitaxial thin film annealed 2 h at 700°C; open circles: observed data points, full line: non-linear least square fit with a Voigt function. The difference line is shown with a separate scale.

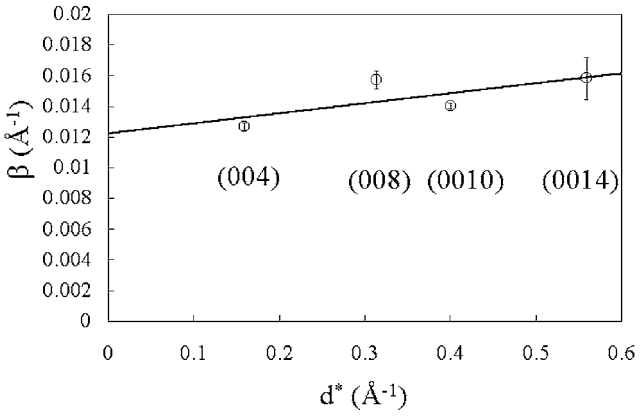

Fig. 4. Williamson–Hall plot of a $SrBi_2Nb_2O_9$ epitaxial thin film annealed 2 h at 700°C; open circles: observed breadths, full line: least square fit.

slowly decaying tails (i.e. strong Lorentzian character) and strong 'order independent' broadening. However, a contribution to microstrains is not excluded since pure 'order independent' broadening is obtained for the extreme case of *infinitely* narrow strain fields [23]. The same tendency has been observed by several authors for analogous mistakes [4–6,24]. They related the apparent domain size D to the contribution of stacking faults D_F using the equation derived by Warren [14] for in-plane translation stacking faults:

$$\frac{1}{\langle D\rangle_s} = \frac{1}{\langle D_c\rangle_s} + \frac{1}{\langle D_F\rangle_s} \qquad (2)$$

where $\langle \ldots \rangle_s$ designates a surface average and D_c is the real crystal size which is related to the film thickness in our case. Hence, knowing the film thickness (approx. 40 nm), Eq. (2) may yield the mean distance between stacking faults. Assuming flat grains of constant thickness, the calculation is straightforward and gives a mean distance between stacking faults $\langle D_F\rangle_s$ of 5 nm for the sample annealed for 30 min. This small value indicates a very high stacking fault density, and in that case the effect of limited film thickness on size broadening is almost negligible, since $\langle D_F\rangle_s \approx \langle D\rangle_s$.

We now consider the shape of the profiles. The average form factor $\langle\phi\rangle$ of the diffraction line has a value of 0.677 for the sample treated 30 min. This figure is close to the Lorentzian limit and agrees well with the presence of planar mistakes [25,26]. Balzar [4] also systematically obtained $\beta_L \gg \beta_G$ in faulted Bi–Cu–O superconductors, with average ϕ values of 0.641, 0.717 and 0.677 depending on the composition.

In a more detailed way, the line shape due to 'size' broadening is almost purely Lorentzian ($\phi_D = 0.670$) whereas microstrains yields a Voigtian line shape ($\phi_e = 0.822$). This is in perfect agreement with the above mentioned model of van Berkum, for high defect densities the 'size' effect is mainly due to stacking faults and the corresponding profile exhibits slowly decaying tails.

The SBN films were annealed at 700°C for durations ranging between 30 min and 500 h. The evolution of the microstructural parameters is given in Table 1; the sample imperfections are noticeably lowered. The column length distribution is depicted in Fig. 5. For a 30-min treatment the distribution is very narrow, with a volume weighted column length of 7.4 (1) nm. When annealing time is increased the domain size increases and the distribution becomes much broader.

The evolution of the form factors $\langle\phi\rangle$ shows that the Lorentzian content of the profile decreases. This is due to the change in shape of the 'size' profile as attested by the increase of the ϕ_D factor. Since stacking faults are responsible for both size effect and Lorentzian shape, these data clearly indicate a lowering of the stacking fault density when annealing duration is increased.

In Fig. 6, the microstrain $\langle e^2\rangle^{1/2}$ is plotted vs. $1/\langle D\rangle_s$. A linear trend with zero intercept is obtained suggesting a film microstructure made of columnar grains divided into regions of a coherent lattice delimited by planar defects [6].

The volume weighted domain size in a sample annealed 500 h at 700°C is 42 (1) nm which approximately equals the film thickness. Obviously, the mean distance between faults calculated using Eq. (2) reaches infinity. Hence samples annealed 500 h at 700°C are almost free of stacking faults; the SBN crystallites have reached an equilibrium state.

Table 1
Results of line profile analysis[a]

	$\langle D\rangle_v$ (nm)	$\langle D\rangle_s$ (nm)	η (%)	$\langle e^2\rangle^{1/2}$ (%)	ϕ_D	$\langle\phi\rangle$
30 min	7.4 (1)	4.1 (1)	3.1 (1)	0.89 (3)	0.670	0.677
2 h	8.0 (1)	5.2 (1)	2.1 (1)	0.60 (2)	0.714	0.719
500 h	42 (1)	31 (1)	0.29 (2)	0.096 (3)	0.746	0.733

[a] $\langle D\rangle_v$ and $\langle D\rangle_s$ are the volume and surface weighted domain size calculated with the Langford and the Warren–Averbach method, respectively. η is the apparent strain calculated with the Langford method, and $\langle e^2\rangle^{1/2}$ is the root mean squared strain calculated with the Warren–Averbach method at $\langle D\rangle_s/2$. The average shape factor $\langle\phi\rangle$ and the shape factor of the size profile ϕ_D are given in the two last columns. The film thickness is approximately 40 nm (estimated from the sol–gel parameters) which agrees perfectly with the 42-nm domain size obtained for 500 h annealing.

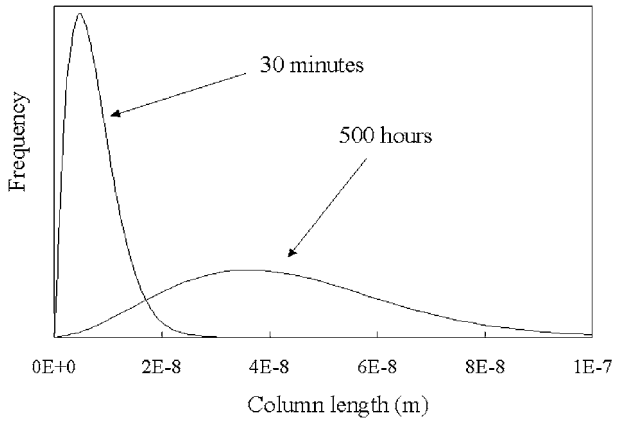

Fig. 5. Domain size distribution calculated with the Warren–Averbach method for two different annealing conditions (30 min and 500 h at 700°C).

5. Conclusion

$SrBi_2Nb_2O_9$ [001] oriented epitaxial thin films have been synthesized by sol–gel processes. After thermal annealing at 700°C for a short duration, those films are shown to exhibit a high stacking fault density. Stacking faults give rise to significant diffraction line broadening as well as marked Lorentzian character.

The film consists of columnar grains divided into regions of coherent diffraction separated by planar faults. The stacking fault density can be reduced by increasing annealing duration at a given temperature. For a 500-h treatment the column length distribution is rather broad; the volume averaged domain size equals the film thickness indicating that the samples are almost free of stacking faults. It is thus possible to obtain stable epitaxial SBN by adjusting the thermal treatment duration. The high sensitivity of XRD to sample imperfections, especially the way in which line breadth and shape are modified by the presence of stacking mistakes, allows reliable and non-destructive process control during the fabrication of thin films.

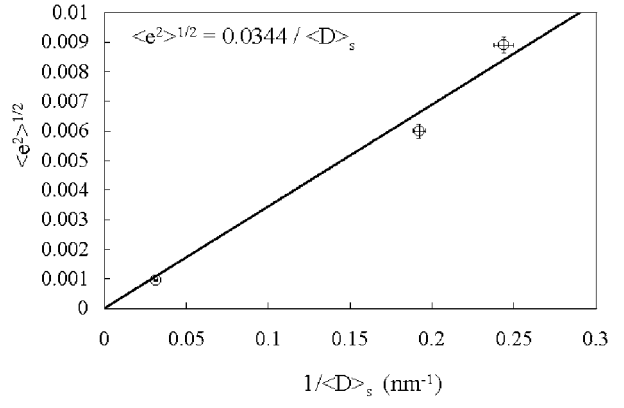

Fig. 6. Plot of the root mean squared strain vs. the reciprocal surface averaged domain size. The zero intercept straight line attests a columnar structure.

References

[1] S.B. Desu, D.P. Vijay, Science 246 (1989) 1400.
[2] B. Aurivillius, Arkiv. Kemi. 1 (1949) 463.
[3] A. Boulle, C. Legrand, P. Thomas, R. Guinebretière, J.P. Mercurio, A. Dauger, Proceeding of the 7th European Powder Diffraction Conference, Barcelona, Spain, May 20–23, 2000, Material Science Forum, to be published.
[4] D. Balzar, J. Res. Natl. Inst. Stand. Technol. 98 (1992) 321.
[5] P. Scardi, L. Lutterotti, L. Correra, S. Nicoletti, J. Mater. Res. 8 (11) (1993) 2780.
[6] P. Scardi, F.C. Matacotta, V.I. Dediu, L. Correra, J. Mater. Res. 12 (1) (1997) 28.
[7] A.I. Ustinov, in: R.L. Snyder, J. Fiala, H.J. Bunge (Eds.), Defect and Microstructure Analysis by Diffraction, International Union of Crystallography, Oxford University Press, New York, 1999, p. 264.
[8] X. Du, I.W. Chen, J. Am. Ceram. Soc. 81 (12) (1998) 3260, 3265.
[9] O. Masson, R. Guinebretière, A. Dauger, Mater. Sci. Forum 278-281 (1998) 115.
[10] R. Guinebretière, A. Dauger, O. Masson, B. Soulestin, A. Dauger, Phil. Mag. A. 79 (7) (1999) 1517.
[11] H.P. Klug, L.E. Alexander, X-Ray Diffraction Procedures for Polycrystalline and Amorphous Materials, John Wiley, New York, 1974.
[12] J.I. Langford, J. Appl. Cryst. 11 (1978) 10.
[13] J.I. Langford, J. Res. Natl. Inst. Stand. Technol. 98 (1993) 321.
[14] B.E. Warren, X-Ray Diffraction, Addison-Wesley, 1969.
[15] A.R. Stokes, Proc. Philos. Soc. Lond. Ser. A 61 (1948) 382.
[16] S. Enzo, G. Fagherazzi, A. Benedetti, S. Polizzi, J. Appl. Cryst. 21 (1988) 536.
[17] P. Scardi, D.C. Kothari, L. Guzman, Thin Solid Films 195 (1991) 213.
[18] D. Balzar, J. Appl. Cryst. 25 (1992) 559.
[19] R. Delhez, E.J. Mittemeijer, J. Appl. Cryst. 9[3] (1976) 233.
[20] E.F. Bertaut, Acta Cryst. 3 (1950) 14.
[21] C. Legrand, J.H. Yi, P. Thomas, R. Guinebretière, J.P. Mercurio, J. Eur. Ceram. Soc. 19 (1999) 1379.
[22] G.K. Williamson, W.H. Hall, Acta Metall. 1 (1953) 22.
[23] J.G.M. Van Berkum, R. Delhez, Th. H. de Keijser, E.J. Mittemeijer, Acta Cryst. A 52 (1996) 730.
[24] D. Balzar, H. Ledbetter, J. Mater. Sci. Lett. 11 (1992) 1419.
[25] A.J.C. Wilson, X-Ray Optics, 2nd ed., Methuen, London, 1962.
[26] C.J. Nuttall, P. Day, J. Sol. Stat. Chem. 147 (1999) 3.